Electronic Supplementary Material (ESI) for Nanoscale.
This journal is © The Royal Society of Chemistry 2015

Moving graphene devices from lab to market: advanced graphene-coated nanoprobes

Fei Hui[1],Pujashree Vajha[1],Yuanyuan Shi[1], Yanfeng Ji[1], Huiling Duan[2], Andrea Padovani[3], Luca Larcher[3], Xiao-Rong Li[4], Jing-Juan Xu[4], Mario Lanza[1*]

[1]Institute of Functional Nano & Soft Materials, Soochow University, 199 Ren-Ai Road, Suzhou, 215123,China. [2]State Key Laboratory for Turbulence and Complex System, Department of Mechanicsand Engineering Science, CAPT, College of Engineering, Peking University, Beijing 100871, China.[3]DISMI, Università di Modena e Reggio Emilia, 42122 Reggio Emilia, Italy. [4]State Key Laboratory of Analytical Chemistry for Life Science, School of Chemistry and Chemical Engineering, Nanjing University, Nanjing 210093, China.

* Corresponding author e-mail: mlanza@suda.edu.cn

Pricing of some of the most used nanoprobes used in AFM research

	Manufacturer	Model	Bulk material	Tip side coating	Radius (nm)	Unit Price (USD)
1	Nanoworld	NCH	Si	None	< 8	37.26
2	Olympus	OMCL-AC240	Si	Pt	15	77.44
3	Bruker	SCM-PIC	Si	Pt-Ir	20	68.61
4	Nanoworld	PPP-EFM	Si	Pt-Ir	20	51.84
5	μ-Masch	NSC/TIPT	Si	Ti-Pt	10	32.40
6	Bruker	MESP	Si	Co-Cr	20	83.86
7	Budgetsensors	Electri Tap 190-G	Si	Cr-Pt	< 25	37.26
8	Bruker	DDESP-FM	Si	Doped diamond	100 - 150	217.29
9	Nanoworld	CDT-FMMR	Si	Doped diamond	< 200	145.81
10	Rocky Mountain	RMN-25PT300B	Pt	None	< 20	121.98
11	Bruker (IMEC)	SSRM-DIA	Diamond	None	5 - 20	579.34

Table S1: Unit price of AFM tips from different manufacturers and with different properties. The radius value is typical and the prices are calculated dividing the price of the smallest box provided by the manufacturer (in Shanghai retailing offices) by the number of tips per box.

Fabrication process

The graphene sheets and graphene solution have been fabricated following the process described in the methods section of the manuscript. The aim of this section is to comment some experimental details that may improve the process, as well as to corroborate that the fabricated graphene-coated tips are suitable for AFM research.

When we started this project, the main concern was how to develop a method to ensure that graphene sheets are always attached to the tip apex. Despite we immediately observed that the sharp shape of the tip can easily trap the graphene sheets, at the beginning we noticed some uncertainty. For the first 5 tips fabricated, one of them didn't show graphene attached to the tip apex in SEM images. To avoid this problem, we intentionally tuned the density of graphene sheets in solution until reaching conformal coating in all the next 10 tips fabricated. Therefore, the density of graphene in solution is critical, and we achieved the best performance mixing 5 mg graphene in 1mL pure water and sonicating the solution for 10 minutes.

After coating the tips, another concern was how the presence of graphene would affect the laser reflection on the back side (if the laser doesn't arrive to the photodiode, the AFM measurement cannot be done). We corroborated that all graphene-coated tips provided high SUM signals to the photodiode (Figure S1a), similar to those of uncoated tips, making possible their use in the AFM. To analyze this phenomenon deeper, we intentionally coated one AFM tip with a larger amount of graphene sheets, and in that case we observe that the SUM signal in the photodiode was remarkably reduced (Figure S1b). All the tips used in the manuscript showed signals similar to Figure S1a.

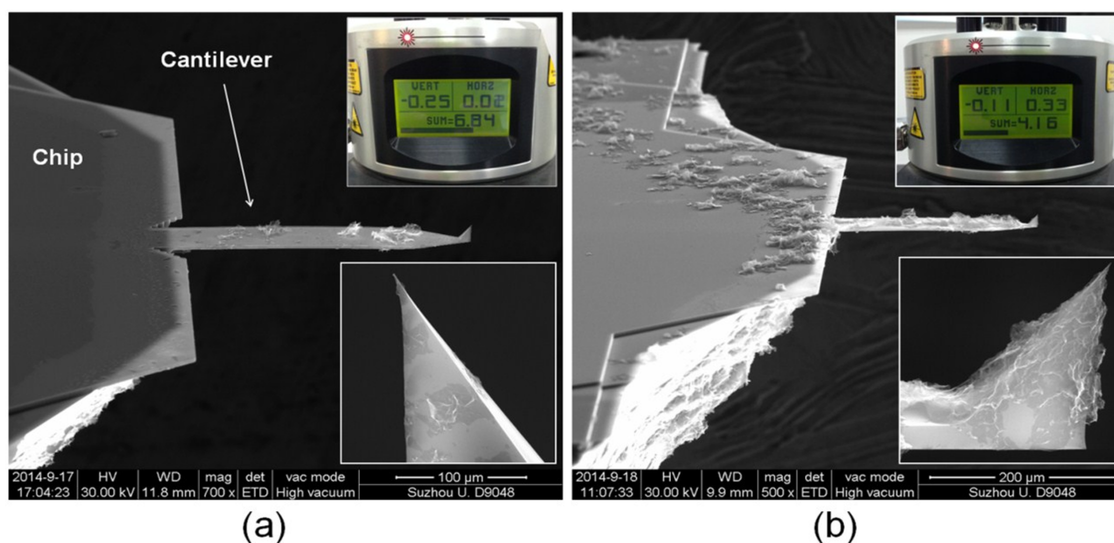

Figure S1: SEM images and SUM signal (top right insets) of OMCL-AC240 tips coated with low (a) and high (b) concentrations of graphene in solution. An excess of graphene on the tip may led to prohibitive reduction of the SUM signal. The SUM values for uncoated tips are typically 8.

Another important point was how to coat the tips without manipulating them. All graphene-coated tips used in the manuscript were fabricated by holding them with the tweezers and immersing them in a small tube containing the graphene solution (one by one). Although this methodology allows rapid and high quality fabrication, manipulation of the AFM tips with the tweezers unavoidably leads to damage on the chip that contains the cantilever (Figure S2a). Despite this doesn't damage the cantilever or the tip, commercializing nanoprobes with scratched tips is not suitable. In order to avoid single tip manipulation and accelerate the process, we optimized the graphene coating step following some easy steps:

i) We removed the transparent cover of the box of tips provided by the manufacturer. ii) We cleaned the box and immersed it (with the AFM tips inside) in alcohol for 3 minutes to remove impurities. The inside part of the box is made of a sticky material that impedes the movement of the tips. These boxes are specially designed to avoid tip damage during shipping, and are provided by all AFM tips manufacturers. We took advantage of this capability and immersed the whole box containing the AFM tips in alcohol, and we observe that the tips don't detach even after immersion in the liquid (Figure S2b). iii) We immersed the box with the AFM tips in pure water for 1 minute, and after that we dried them with a N_2 gun using a low gas pressure of 0.02MPa (high gas pressures may lead the tips fly away). iv) Once the box was cleaned, we immersed it (containing the AFM tips) in the graphene solution and agitated for 30 seconds. Longer times may lead to unwanted excess of graphene on the tip. v) Finally, we dried graphene-coated tips and box with the N_2 gun. We also observed that blowing the graphene-coated tips with the N_2 gun improved the adhesion of the graphene sheets to the tip apex, as well as it can even remove unwanted excess of graphene on the tips.

Using this methodology, we achieved conformal coating for a whole box containing 10 AFM tips in less than 5 minutes without the need of single tip manipulation. The amount of graphene sheets in solution can be considered inexhaustible, and the process could be repeated using the same solution. It is worth noting that, when exported to the industry, the graphene-coating step could be further improved. Ideally, it should be done before placing the chips on the sticky box. The bath in graphene solution and drying with N_2 steps could be easily automated, avoiding human labor and accelerating the whole process, which would improve the quality and reduce the production costs. Therefore, this methodology may be very competitive for the industry.

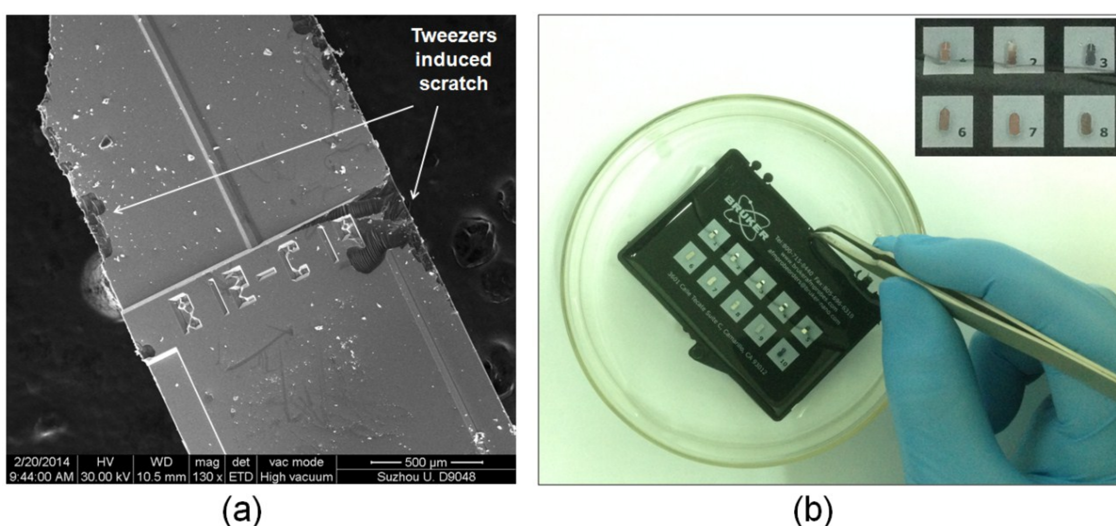

Figure S2: (a) SEM image of the chip that holds the cantilever and AFM tip after manipulating it with the tweezers. The image shows unavoidable damage at the edges. (b) Photograph of a box containing AFM tips partially immersed in pure water. The sticky box provided by the manufacturer can hold the tips even after immersed in the liquid, allowing the graphene-coating step without need of single chip manipulation.

<u>Variability analysis</u>

As all devices, our graphene nanoprobes also show deviations. But we believe the important thing is how much these deviations influence the value of the measurement performed compared to other experimental parameters, as well as how do they affect the performance of the whole device. In the following, we explain the variability produced by the main parameters involved in a CAFM measurement, and we compare it to the effect of the deviations produced by different graphene coatings.

First of all, we have to say that the fabrication of nanoprobes is a process highly affected by deviations. The best way to display this is just to put an eye on the specifications provided by the manufacturer:

Parameter	Typical	Maximum	Minimum
Spring constant (N/m)	2	0.6	4.6
Resonant frequency (kHz)	70	95	45
Tip radius (nm)	15	---- Less than 25 nm -----	
Metal coating thickness (nm)	20	10	30
Tip height (µm)	14	9	19

Table S2: Specifications for the main nanoprobe used in this work, the OMCL-AC240-TM from Olympus. The data have been extracted from reference [ref. S1].

On the other hand, in a CAFM system, the measurements are strongly affected by many different experimental factors, such as relative humidity, external forces and sample stiffness, among others. In order to quantify them we can ensure that, the currents measured by the nanoprobe in a CAFM system correspond to:

$$I = J \cdot A_c \qquad (1)$$

where, J is the current density and A_c is the tip/sample contact area. In our experiments, the conduction thought the nanojunction formed by the metal-varnished AFM tip and the GSL/Cu test sample is, linear (as it can be seen in the blue lines of Figures 2d and 3d of the manuscript). Therefore I could be expressed as:

$$I = V \cdot \alpha \cdot A_c \qquad (2)$$

where α is a parameter linked to the intrinsic resistivity of the tip/sample junction. According to the Hertz contact theory, which is the most used to study interactions between the tip and the sample in AFM systems [ref. S2-S5], A_c can be quantified as:

$$A_c = \pi \cdot r^2 = \pi \left(\frac{F_c R_{tip}}{K}\right)^{2/3} \text{with } \frac{1}{K} = \frac{3}{4}\left(\frac{1-v_1^2}{E_1} + \frac{1-v_2^2}{E_2}\right) \qquad (3)$$

where r_c is the contact radius (the radius of the contact area), F_c is the contact force between the tip and the sample, R_{tip} is the tip radius and $E_{1/2}$ are the elasticity moduli and $n_{1/2}$ are the Poisson ratios of the tip and the sample. And the F_c is given by the Hooke's law [ref. S6], which is:

$$F_c = -k_c \cdot \delta_c + F_{ext} \qquad (4)$$

where k_c is the spring constant of the tip and δ_c is the deflection of the tip and Fext is the sum of external forces, such as capillary forces, electrostatic forces and others [ref. S7].

Taking all this in mind, we can compare the effect of different parameters on the CAFM measurement of the current. Different amounts/layers of graphene would have an important effect on the radii and imaging/spectroscopic measurements, but we can certainly ensure that this is going to be much lower than the standard deviations of the values provided by the

manufacturer. For example, if we consider an AFM tip coated with 1 layer or graphene and another one coated with 5 layers of graphene, compared to the uncoated tip, the first would have increased its radius in 0.46 nm, which is the thickness of a graphene film produced by this method [ref. S8], while the second one will have increased its radius in: 5 · 0.46 nm = 2.3 nm. Please see Figure S3 (a-c) for a better understanding. It is worth noting that it is highly improbable to achieve conformal coating if 5 independent sheets of monolayer graphene attach to the nanoprobe. Therefore, as our images clearly demonstrate conformal coating for all the tips (Figure 1 of the manuscript), we can ensure that even this maximum hypothetical deviation is much lower than the intrinsic tip-to-tip variability indicated by the manufacturer, who gives a typical radius of 15 nm and a maximum of 25 nm.

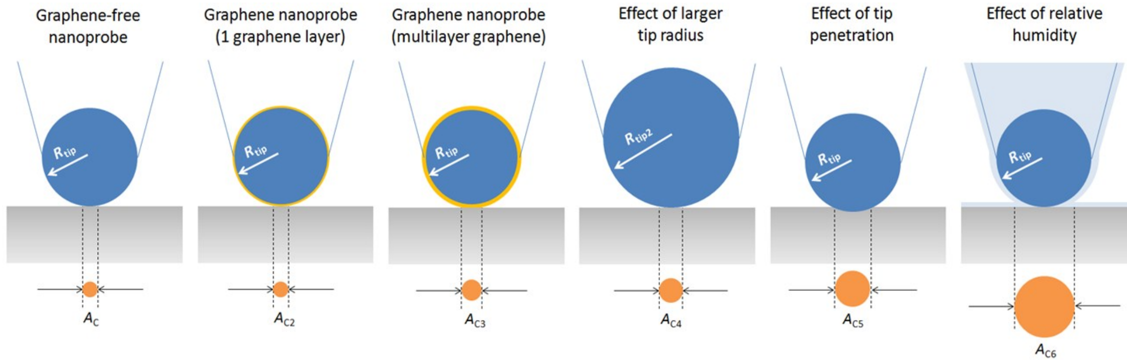

Figure S3: Schematic of the different experimental values that affect the a CAFM measurement.

Moreover, the AFM tips used in our experiment show spring constant deviations up to 20% (Table S2), which can remarkably alter the contact force between the tip and the sample, modifying the tip/sample contact area and the current measured by the CAFM [ref. S9]. In order to display this effect, Figure S4 shows 25 IV curves measured with different graphene-free nanoprobes at different locations of the sample, but using a similar deflection setpoint. As it can be observed, despite the currents are always linear they can vary up to a factor between 13 and 76. Frammelsberger et al. [ref. S9] indicating that differences on the contact force (produced by different spring constants) could lead to variations on the contact area up to a factor 20.

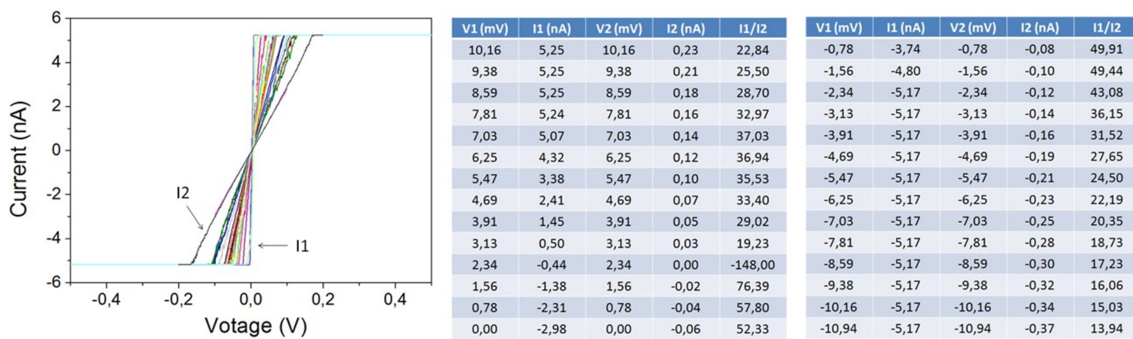

V1 (mV)	I1 (nA)	V2 (mV)	I2 (nA)	I1/I2
10,16	5,25	10,16	0,23	22,84
9,38	5,25	9,38	0,21	25,50
8,59	5,25	8,59	0,18	28,70
7,81	5,24	7,81	0,16	32,97
7,03	5,07	7,03	0,14	37,03
6,25	4,32	6,25	0,12	36,94
5,47	3,38	5,47	0,10	35,53
4,69	2,41	4,69	0,07	33,40
3,91	1,45	3,91	0,05	29,02
3,13	0,50	3,13	0,03	19,23
2,34	-0,44	2,34	0,00	-148,00
1,56	-1,38	1,56	-0,02	76,39
0,78	-2,31	0,78	-0,04	57,80
0,00	-2,98	0,00	-0,06	52,33

V1 (mV)	I1 (nA)	V2 (mV)	I2 (nA)	I1/I2
-0,78	-3,74	-0,78	-0,08	49,91
-1,56	-4,80	-1,56	-0,10	49,44
-2,34	-5,17	-2,34	-0,12	43,08
-3,13	-5,17	-3,13	-0,14	36,15
-3,91	-5,17	-3,91	-0,16	31,52
-4,69	-5,17	-4,69	-0,19	27,65
-5,47	-5,17	-5,47	-0,21	24,50
-6,25	-5,17	-6,25	-0,23	22,19
-7,03	-5,17	-7,03	-0,25	20,35
-7,81	-5,17	-7,81	-0,28	18,73
-8,59	-5,17	-8,59	-0,30	17,23
-9,38	-5,17	-9,38	-0,32	16,06
-10,16	-5,17	-10,16	-0,34	15,03
-10,94	-5,17	-10,94	-0,37	13,94

Figure S4: (left) 25 IV curves measured by different graphene-free nanoprobes. (right) table displaying the voltage and current for the most and less conductive IV curves (IV1 and IV2 respectively). The ratio between I1 and I2 is also displayed.

It is also true that different amount/layers of graphene on two tips within the same box would also produce a shift on the current, as that may modify the factor α in equation (2). To analyze this point, we compare 25 IV curves measured with different standard and graphene-coated. The results can be observed in Figure S5, which indicates that the deviations are negligible.

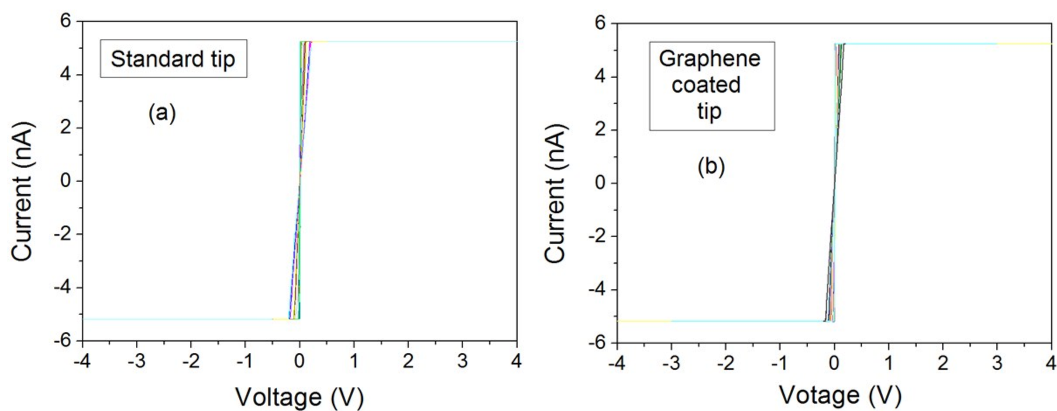

Figure S5: (a) 25 IV curves collected at different locations of the sample with different standard (a) and graphene-coated (b) nanoprobes. (b) The variability is very similar for both tips.

We would like to highlight that, even when using the same tip at the same location of the sample, some reasonable deviations related to the experimental setup appear in the IV curves, and they are always much larger than those introduced by our graphene coating. As an example, Figures S6a and S6b show different IV curves sequentially measured at the same location of the sample for the ame standard and a graphene-coated nanoprobe (respectively). As it can be observed, the variability of a graphene nanoprobe is even slightly smaller.

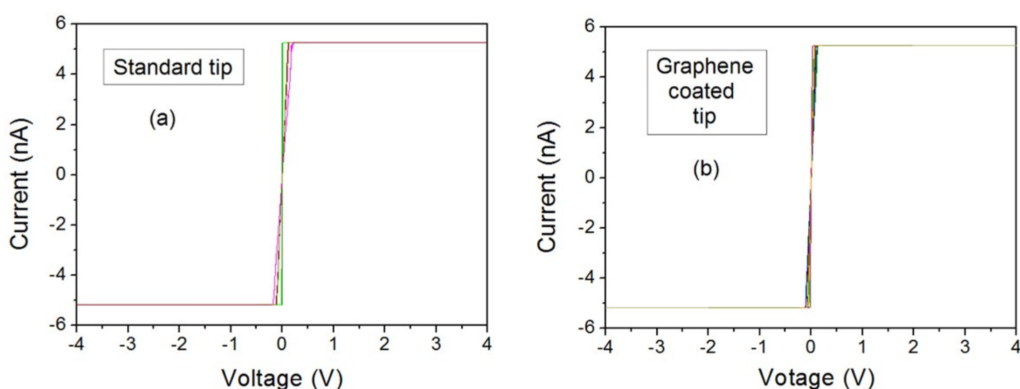

Figure S6: (a) 8 IV curves collected sequentially with one standard nanoprobe at one location of the sample (b) 15 IV curves collected sequentially with one graphene-coated nanoprobe at one location of the sample.

Finally, we would like to highlight that the graphene sheets attached to the cantilever and side parts of the tip cone (not apex) contain wrinkles. We would like to highlight that the metal-varnished tip was already highly conductive before the coating, and that the graphene-coating has only one goal: protect the tip apex. Therefore, the formation of wrinkles on the graphene attached to the sides of the tip doesn't have any effect on the currents measured for two reasons:

1) Once the electrons flow from the sample to the tip (through the graphene), they can disperse along the whole geometry of the tip, moving along the metallic varnishThe current cannot flow along the graphene, as the flakes don't fully cover the geometry of both the tip and the cantilever
2) Even if scattering effects could be introduced, the area of the tip covered by wrinkles is much smaller than that of wrinkle-free or graphene-free parts, which are higly conductive.

Also, please note that the effect of wrinkles will never have an effect as large as that of the experimental factors described in the previous comment.

Ageing characterization

To characterize the performance of the AFM tips, we use a three step methodology that ensures real imaging (Figure S7). It is known between fabrication and first use, native oxides can grow on the metallic varnish of the tips, which may lead to false imaging. To avoid this problem, in the first step we apply sequences of I-V curves with the CAFM, using low end ramp voltages and progressively increasing until the current during the backward curve becomes Ohmic.

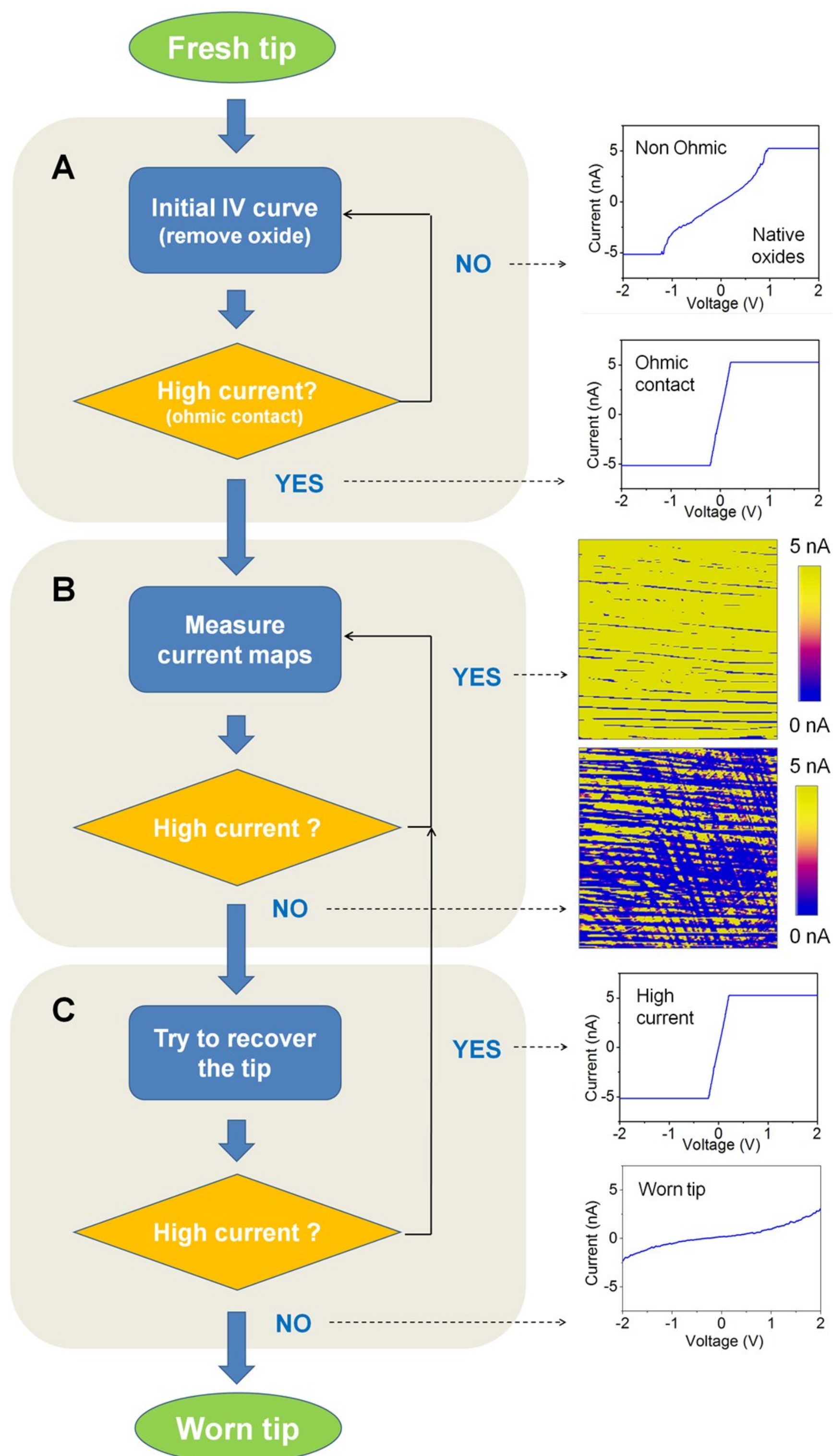

Figure S7: Flux diagram of the process used to characterize the electrical properties of the tips.

Usually, end ramp voltages of 0.5V are enough to break the native oxide. Once the native oxide is broken and ohmic current is observed, we start a sequence of topography and current maps (simultaneously collected). At the beginning of this investigation, we needed to find out the most suitable parameters that can generate tip damage in a reasonable time. After trying different combinations, we found that a deflection setpoint of 4V and a bias of 1V are the parameters that best display the tip wearing. Such parameters don't produce sample damage, as corroborated in Figures S10a and S10o. It should be noted that, for all the tips, the first scan performed on a fresh location of the sample has been collected with a bias of 3V to remove possible oxides on the sample. After that, sequences of current maps using 1V have been applied until observing tip wearing. We compare all current images with the same current scale to display better the changes of the conductivity. Once conductivity reduction has been observed, we need to make sure that it comes from the tip varnish wearing, and not from particle/oxide adhesion to the tips. This is a common phenomenon in AFM research. To do so, we apply sequences of I-V curves, similar to the first step, and try to observe conductivity increase. If the tip doesn't show conductivity recover, which probably means that the tip varnish is melted, as corroborated by SEM images (Figure 2c). On the contrary, sometimes the tip conductivity was recovered, and then we kept measuring current maps. This methodology ensures a correct display of the tip properties.

As it can be observed in Figure S7, the currents in the I-V curves saturate at ± 5 nA. This is related to the electronics of the AFM, and happens in almost all CAFMs, including the Bruker Dimension Icon, Digital Instruments 3100, Omicron, Nanotec, Park XE-100, Agilent 5500, and NT-NDT (see our previous publications [ref. S10-S13]). For all these equipments, the maximum currents measured using the standard electronics provided by the manufacturer never surpass 100 nA. The main reason is that all manufacturers use linear current-to-voltage preamplifiers (the current measured by the tip needs to be converted into voltage before sending it to the computer, so that it can be read by the data acquisition card). In order to visualize larger currents, we removed the linear I-V preamplifier and connected an external Keithley 2400 sourcemeter to the tip and sample. The whole setup and connections can be observed in Figures S8a and S8b, respectively.

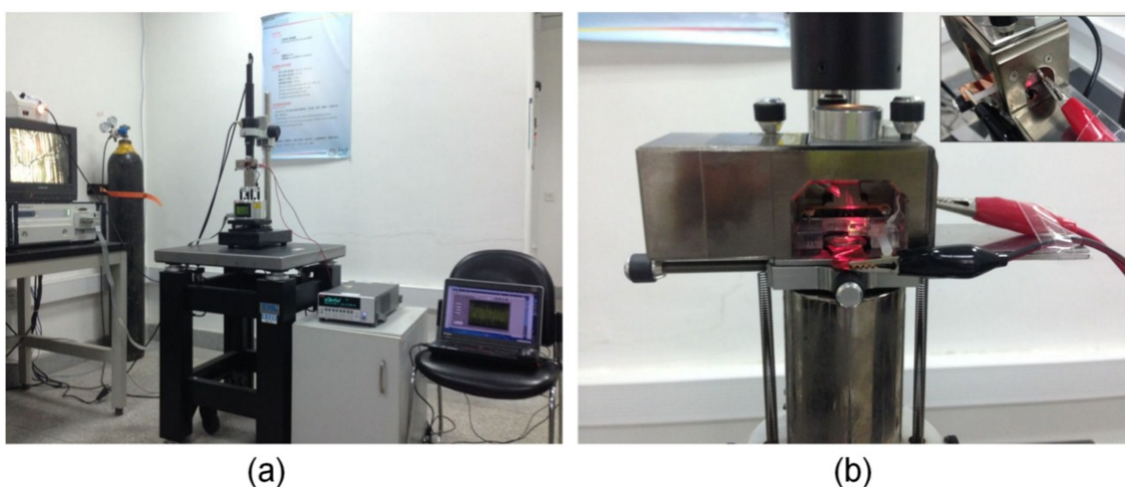

Figure S8: (a) Enhanced setup used for measuring the I-t curves. (b) Detail of the connections between the sourcemeter and the AFM tip and sample plate.

To remotely control the sourcemeter and store the I-V curves, we connected it to a computer using the Keithley KUSB-488B GPIB-USB cable. Initially, we used the free software provided by the manufacturer to control the sourcemeter (Labtracer 29), but the capabilities provided were very limited (it only allows measuring I-V curves, not I-t, and it doesn't allow selecting parameters such as final I-V curve time and step time). To avoid this limitation, we designed a

custom software in Labview that allows measuring I-t curves selecting the voltage, step time, number of steps and current limitation (see Figure S9). For the I-t curves shown in Figure 4b of the manuscript, we selected a current limitation of 10 mA, which was never reached. The noise level of this setup is up to some nanoamperes, but it may be further improved using the another sourcemeter (such as the Keithley 6430 Sub-Femtoamp Remote Sourcemeter) [see ref. 22 manuscript].

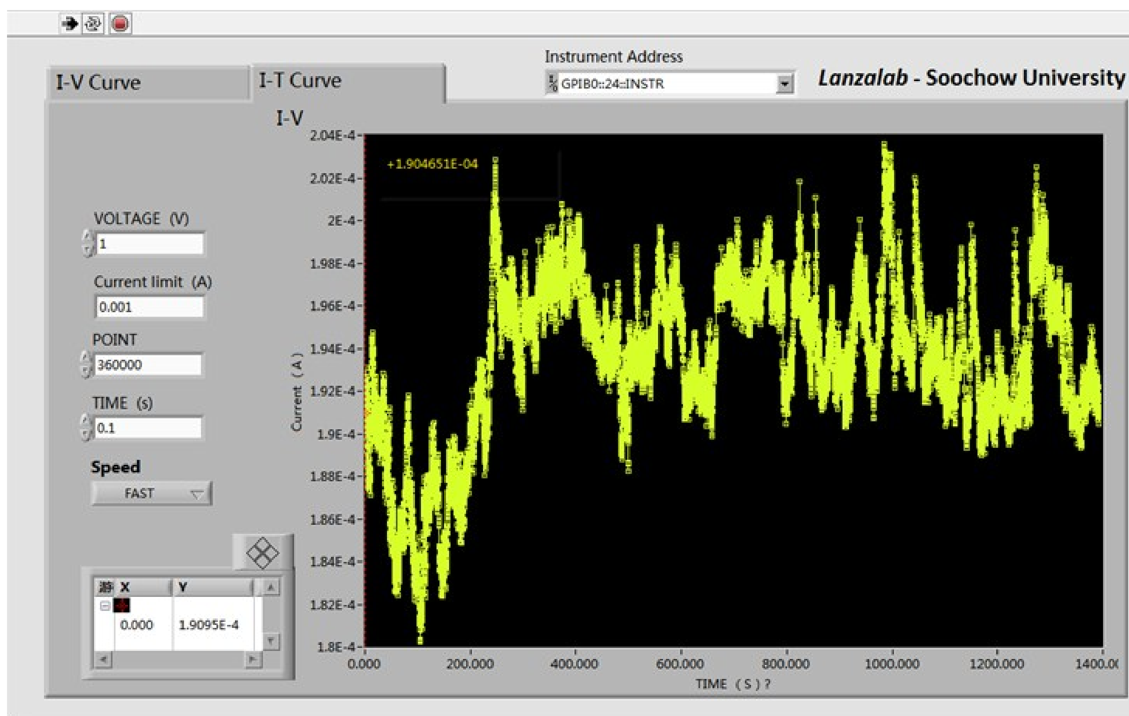

Figure S9: Layout of the custom-designed Labview software used to remotely control the sourcemeter and store the data from the I-t curves.

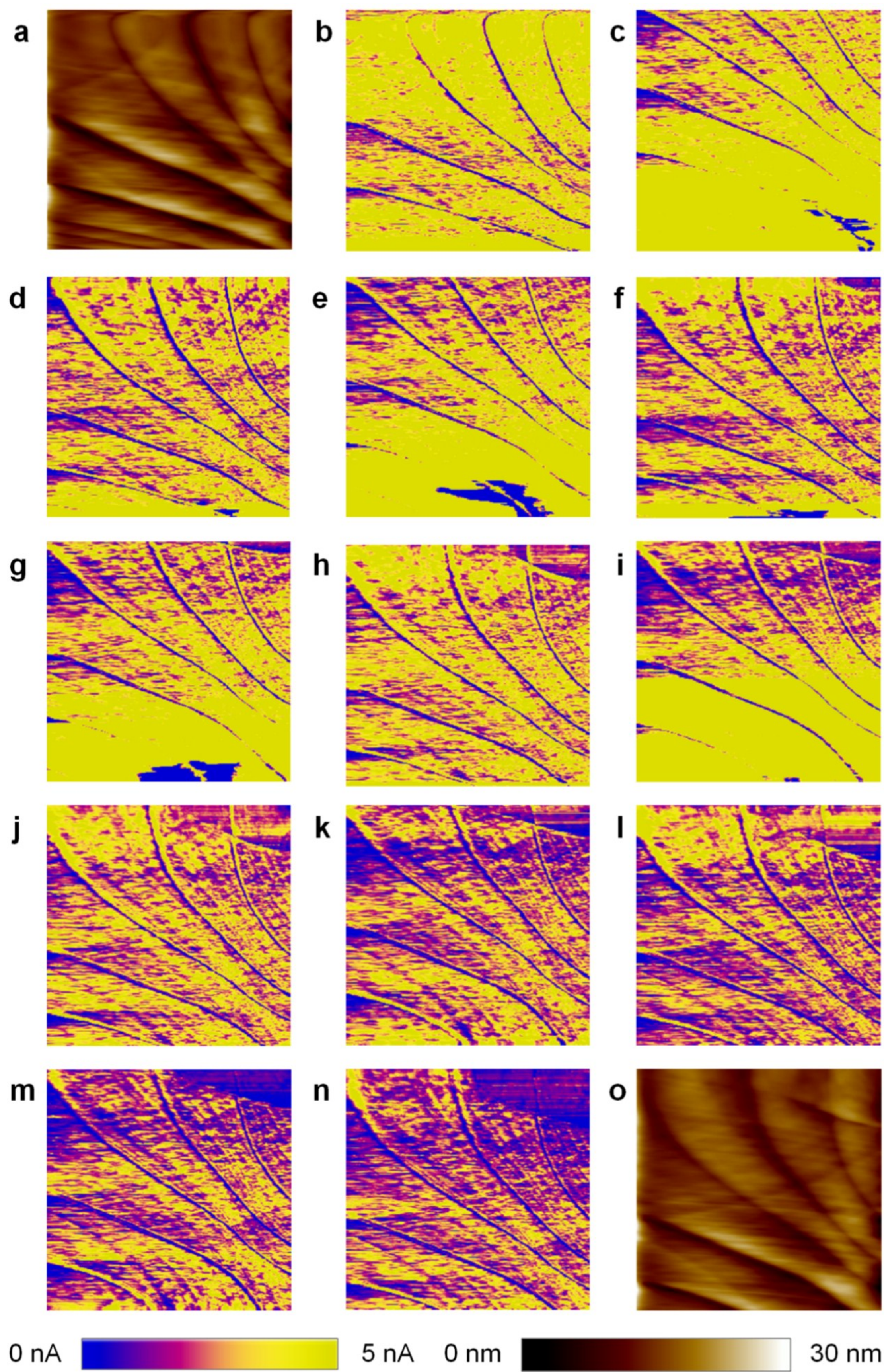

Figure S10: Halfway current scans between the two inset maps in Figure 2a of the manuscript. The first and last topographic maps are also displayed, and they show that the tip doesn't alter the sample. All images are 4μm x 4 μm.

Comparison to doped-diamond varnished silicon tips

It is important to remark that the selection of the tip is critical in AFM research. As mentioned in the manuscript, the most stable conductive nanoprobes one can find in the market are doped-diamond varnished and solid diamond tips. These nanoprobes are indicated for applications that require very high contact forces, such as Scanning Spreading Resistance Microscope (SSRM), Scanning Capacitance Microscopy (SCM) and static Tunneling/Conducting AFM. Despite having very large lifetimes, it is known that these tips may not be suitable for some applications. Blasco et al. [see ref. 29 manuscript] corroborated that, due to their large radius, when characterizing the local properties of thin oxides the resolution of doped-diamond varnished tips was much smaller than that of Pt-varnished ones, leading to difficult recognition of the typical features of the samples, such as conductive spots and grain boundaries. We corroborated this observation. Figures S11a and S11b show, the topographic and current images obtained when measuring a SLG/Cu stack with a doped-diamond tip. As it can be observed, the lateral resolution of the images obtained with diamond tips is lower when displaying size of the steps, and the topographic images obtained with graphene-coated tips are much clear even after several scans. The reason is the larger tip radius of doped-diamond tips, which ranges between 100 nm and 200 nm.

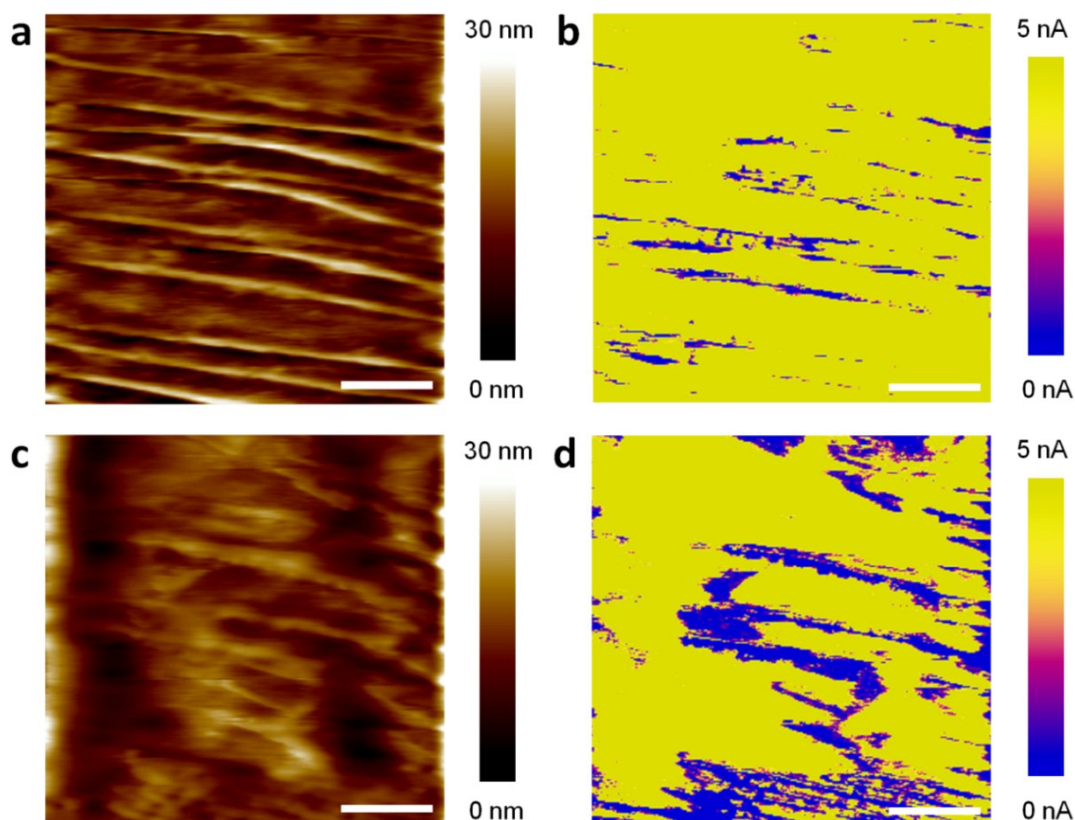

Figure S11: First (top) and 23rd (bottom) topographic (a, c) and current (b-d) scans using a doped-diamond varnished tip. The ageing of the tip is evident from the maps.The scale bars in all images are 1 μm.

Additionally, we observe that diamond tips can dramatically abrade the surface of the sample (Figure S11c). It is worth noting that the doped-diamond AFM tips used in this experiment have a nominal spring constant of 6.2 N/m, three times larger than that of the metal-varnished ones (2 N/m). To discard the effect of the contact force, we used a deflection setpoint four times smaller than that used for Pt-varnished tips (4V for Pt-varnished vs. 1V for doped-diamond). Sample

degradation can be easily explained from the mechanical properties of the varnishes. It is widely known that the Young modulus of the Cu sample is 128 [ref. S14], while the one of the diamond varnish ranges between 900 and 1050 [ref. S15], leading to easy sample surface damage (here the presence of graphene has not been considered because it is flexible and cannot damage the sample, and because its mass is negligible compared to the three dimensional nature of the tip varnish and sample). On the contrary, the Young modulus of the Pt varnish is 170 [ref. S16], closer to the one of the sample, producing less wearing. We repeated the experiments using one of the most used samples in nanotechnology, a piece of n-type Silicon, and again the images collected with doped-diamond tip very poorly show the features of the sample, and generate evident damage.

Furthermore, doped-diamond tips can be also aggressively degraded when measuring softer samples. Surprisingly, we observed that the conductivity of a doped-diamond tip remarkably decreased after scanning an area of 368 μm^2 (Figure S11d). In this case, the conductivity reduction doesn't come from varnish wearing, but from prohibitive adhesion of particles to the tip apex, as corroborated by SEM images (Figure S12). Particle adhesion to the apex of the tips is normal in contact mode AFM research and it has been also observed for graphene-coated tips (Figure 2f), but in that case the amount of particles was remarkably lower even for larger scanned areas. This further corroborates that doped-diamond varnished tips are only suitable for measurements in which the tip remains static of the sample (Figure 2h), or for cases where extremely large forces are required.

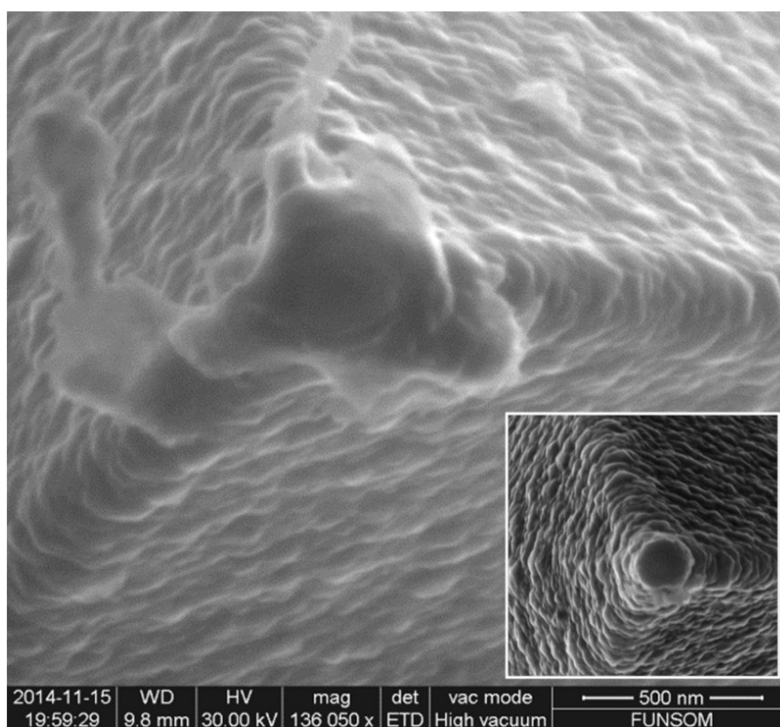

Figure S12: SEM image of an aged doped-diamond varnished AFM tip after scanning 368 μm^2 of a SLG/Cu sample. A particle attached to the apex can be distinguished. The inset shows the initial shape of the tip.

In other words, our graphene-coated tips encompass all wanted capabilities of both metal and doped-diamond varnished tips: they are cheap, sharp, conductive and gentle to the sample as metal-varnished tips, and durable as diamond tips. It is worth noting that AFM tips with such

properties are not available in the market, indicating that this methodology allows fabricating nanotips with customized properties.

Bringing graphene nanoprobes to the limit

When a graphene nanoprobe is exposed to extraordinarily large contact forces, the apex of the tip may break due to the frictions during the scan, but we observe that the graphene flake effectively survived, trapping the detached particle (Figure S13). This methodology could be used in the future to intentionally trap particles or fluids between the tip and graphene sheet and test their mechanical properties.

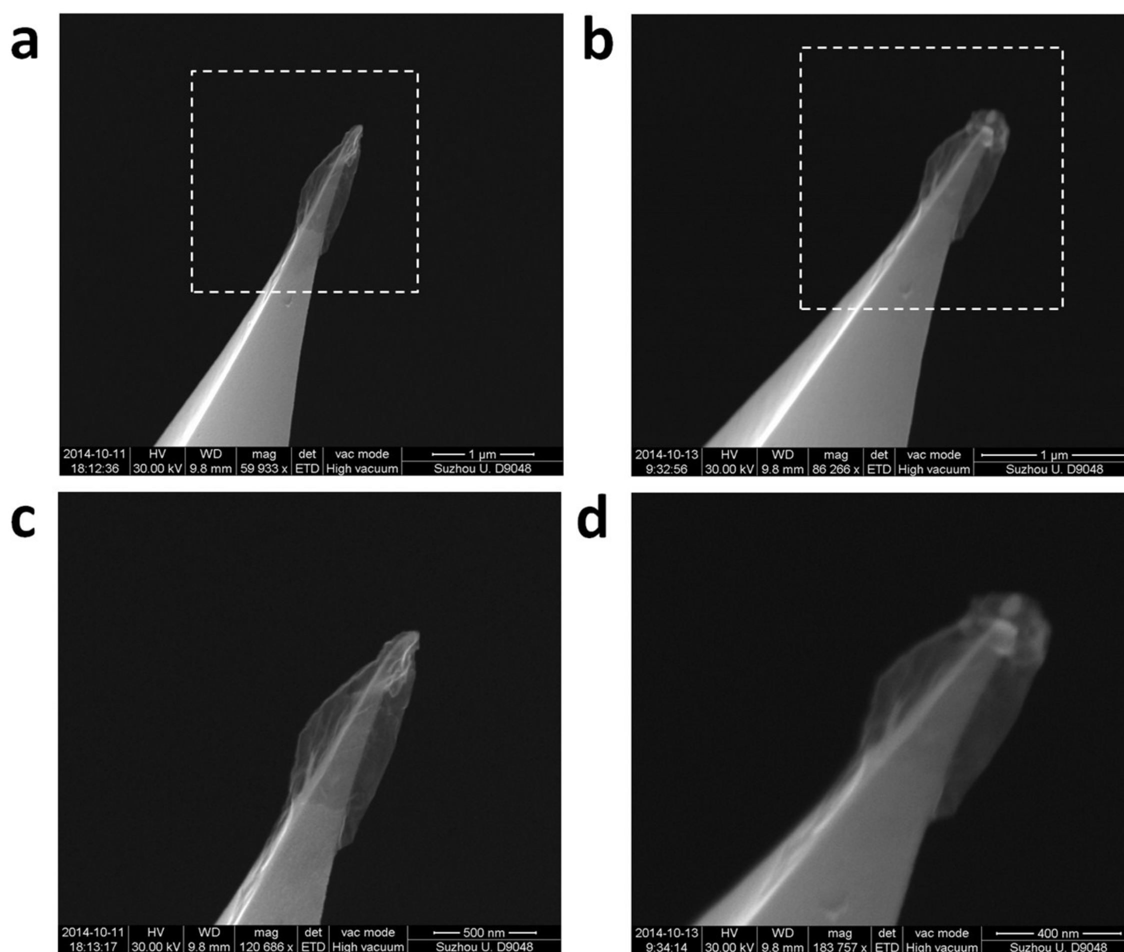

Figure S13: SEM images collected for a graphene nanoprobe (a) before and (b) after AFM experiments. Figures (c) and (d) are the zoom in images of the squared areas shown in (a) and (b), respectively.

Using hydrophobic polymer coatings

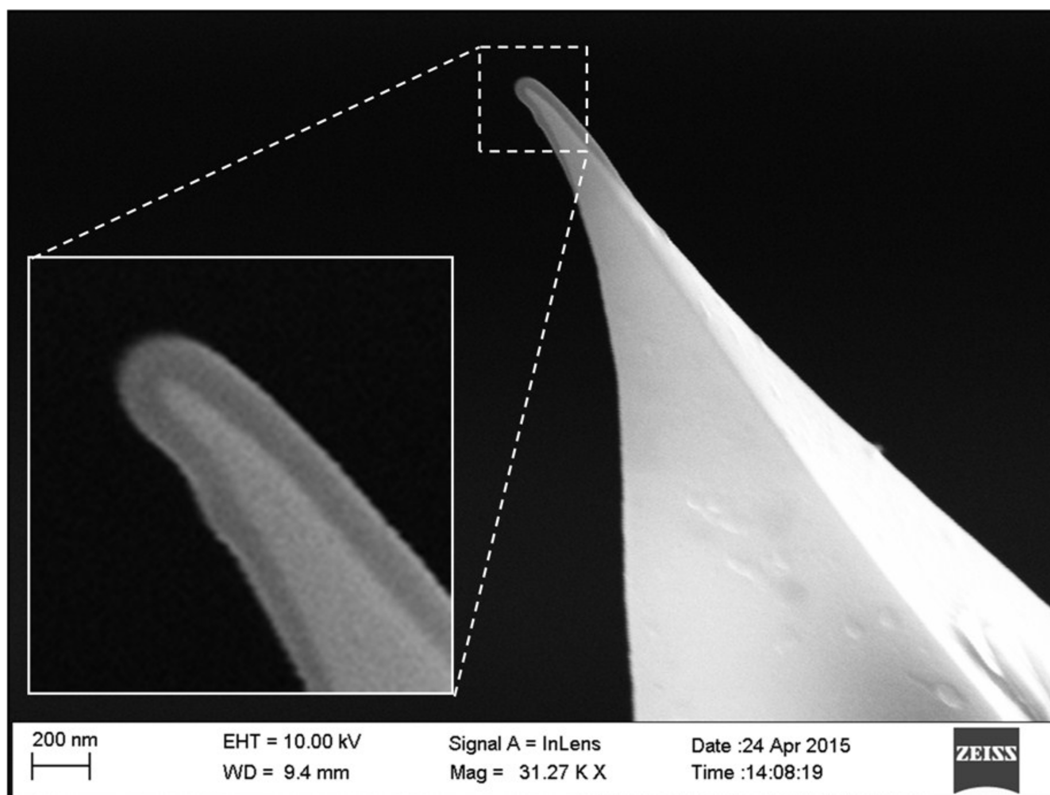

Figure S14: SEM image collected for a standard nanoprobe coated with a ~ 100 nm thickpolymer layer. The dramatic increase on the tip radius, which affects the lateral resolution of the nanoprobe, can be clearly distinguished.

Tunneling current simulation for hydrophilic metal-coated

In order to understand the conductivity changes observed in the I-V curves collected with standard (graphee-free) nanoprobes (Figure 3a of the manuscript), the current through the tip/sample nanojunction has been simulated using the widespread charge transport model reported in [ref. S17-S19]. In this model the gate current includes both direct tunneling (DT) and trap-assisted-tunneling (TAT) contributions. The hole and electron DT currents from the inverted substrate are calculated within the semi-classical approximation [ref. S20], while the electron DT current from the metal gate is computed using the Tsu-Esaki formula [ref. S21]. The tunneling probabilities are calculated through the Wentzel-Kramer-Brillouin (WKB) method. The electric field across the stack is calculated taking into account the charge quantization effects at the H_2O/Si interface [ref. S22] and the carrier freeze-out at low temperature [ref. S12]. The TAT current is calculated by summing up the contributions from the defects forming multiple possible percolation paths [ref. S18] in the water layer. These defects are generated randomly with respect to their energies and position. The current driven through each given conductive path is determined by the slowest trap in the path. More details about the physics related to the model can be found in references [ref. S17-S23].

For the calculation presented in Figure 3b of the manuscript a 15 nm x 15 nm squared Pt/H_2O/Si heterojunction has been generated (Figure S15, left). The size has been chosen to match the typical tip/sample contact area for an AFM working in air environment and using similar tips, which ranges between 100 and 300 nm^2 [ref.S1-S2]. The silicon doping and resistivity are 10^{16} cm^{-3} and 0.3-0.5Ω·cm, respectively. The work function of the Pt has been selected to be 5 to match the properties of the PtIr nanoprobe [olympus], the affinity of the water layer is 0.65 eV and its dielectric constant is 60 [ref. S24-S25]. Then, the current through the structure has been calculated according to the equations described in the model [ref. S17-S23], depending on the potential difference applied between the Pt electrode and the n-Si substrate, and using the H_2O layer thickness as the only variable parameter. We found that, the currents observed in the trace plot (Figure 3b in the manuscript, blue lines), fit to the currents using a thickness of 10 Å, while those in the retrace plot fit to a thickness of 1Å. These differences indicate that during the trace ramp the currents are anomalously small due to the presence of a water layer between the tip and the sample. When the current increases, the electrical field produces an attractive force between the tip and the sample (F_{EL} in Eq.1 of the manuscript), bringing the tip in contact to the sample (1 Å is almost negligible) and leading to a current increase. The absence of such observation using graphene tips indicate that the H_2O layer at the junction is removed due to the hydrophobic nature of the graphene coating.

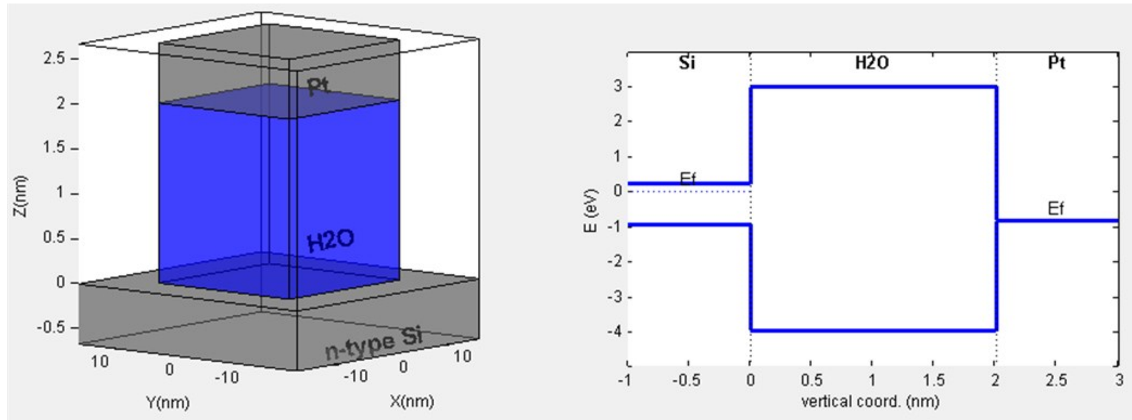

Figure S15: (left) Three dimensional schematic of the nanojnction simulated, with the Pt, H_2O and n-Si layers. (right) corresponding band diagram of the layers before band bending.

Adjustment of the zero-current voltage in the CAFM setup

In order to ensure that no current is generated due to parasitic or offset voltages, we quantified the voltage that produces zero currents for each tip. More specifically, we consider zero currents as those currents below the noise level of the CAFM (1pA). To do so, for each tip I-V curves were collected on a metallic sample, which is similar to the process used by the tip manufacturer to characterize the tip resistance [ref. S26]. All tips showed Ohmic contact similar to that displayed in Figure S15.Interestingly, the zero current doesn't appear for a voltage of 0 mV. In our AFM, for this specific tipthe voltage that produces 0 pA is 2.7 mV, indicating the presence of a small offset in the machine. We have observed that this value slightly changes for each tip (it has ranged between 2.44 mV and 2.76 mV for 14 different tips). For the results shown in Figures 2 and 3 of the manuscript this offset doesn't affect the measurement, as in Figure 2 we are applying a voltage, and in Figure 3 there silicon sample presents an intrinsic much larger potential barrier. But for the piezoelectric experiment in Figure 4 of the manuscript, this offset

should not to be ignored. Thus, before all the piezoelectricity experiments shown in the manuscript, the voltage that produces zero current was applied during the force-distance curves, which discards that the currents measured come from any kind of offset.

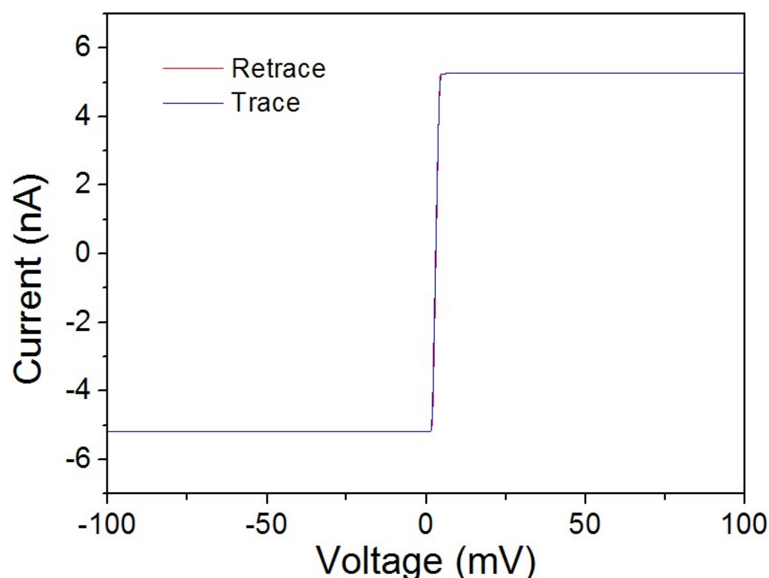

Figure S16: Typical IV curve collected with the CAFM using a metal-varnished tip and a metallic sample. The voltage that produces zero current (less than 1pA) was typically shifted from the 0 mV, and it ranged between 2.44 mV and 2.76 mV for 14 different tips.

ADDITIONAL REFERENCES

[ref. S1] http://probe.olympus-global.com/en/product/omcl_ac240tm_r3/sp.cfm
[ref. S2] Ruskell,T. G.; Workman,R.; Chen,D.; Sarid,D.; Dahl,S.; Gilbert,S. *Appl. Phys. Lett.***1996**, *68*, 9.
[ref. S3] Olbrich,A. “Charakterisierung du¨nner Dielektrika mittels modifizierter Rasterkraftmikroskopie (Characterisation of thin dielectrics by means of modified atomic force microscopy)”, PhD thesis, University of Regensburg, Regensburg, Germany, 1999.
[ref. S4] B. Bhushan (Ed.), Springer Handbook of Nanotechnology, Springer-Verlag, Berlin, 2004.
[ref. S5] A. Born, “Nanotechnologische Anwendungen der Rasterkapazitätsmikroskopie und verwandter Rastersondenmethoden (Applications of scanning capacitance microscopy and scanning probe microscopy techniques in nanotechnology)”, PhD thesis, University of Hamburg, Hamburg,Germany,2000,availablefrom:http://www.physnet.unihamburg.de/services/fachinfo/___Volltexte/Axel___Born/Axel_Bron.htm (accessed in January 18, 2015).
[ref. S6] Louey,M. D.; Mulvaney,P.; Stewart,P. J. *J. Pharm. Biomed. Anal.***2001**, *29*, 559.
[ref. S7] Cappella,B.; Dietler,G. *Surf. Sci. Rep.* **1999**, *34*, 1.
[ref. S8] Lee,D. W.; Hong,T. K.; Kang,D.; Lee,J.; Heo,M.; Kim,J. Y.; Byeong-Su Kim, H. Shin,S. *J. Mater. Chem.***2011**, *21*, 3438.
[ref. S9] Frammelsberger,W.;Benstetter, G.; Kiely, J.; Stamp, R.*Appl. Sur. Sci.***2007**, *253*, 3615.
[ref. S10] Lanza,M.; Porti, M.; Nafria, M.; Aymerich, X.; Benstetter, G.; Lodermeier, E.; Ranzinger, H.; Jaschke, G.; Teichert, S.; Wilde, L.; Michalowski, P. P. *IEEE Trans. Nanotechnol.***2011**,*10*,344.

[ref. S11] Lanza,M.;Porti, M.; Nafria, M.; Aymerich, X.; Whittaker, E.; Hamilton, B.*Microelectron. Reliab.***2010**, *50*, 1312.
[ref. S12] Lanza,M.; Iglesias, V.; Porti,M.; Nafría, M.; Aymerich, X. *Nanoscale Res.Lett.***2011**, *6*,108.
[ref. S13] Iglesias,V.; Lanza, M.; Zhang, K.; Bayerl, A.; Porti, M.; Nafria, M.; Aymerich, X.; Benstteter, G.; Shen, Z. Y.; Bersuker, G. *App. Phy. Lett.***2011,** *99*, 103510.
[ref. S14] Liang, C.; Prorok, B. C. *J. Micromech. Microeng.***2007**, *17*, 709.
[ref. S15] Khurshudov, A.; Kato, K.; Koide, H.*Wear***1997**, *203*, 22.
[ref. S16] Brandes, E.A.; Brook, G.B. Smithells Metals Reference Book, 7th ed., Butterworth-Heinemann, Oxford, Table 15.1. (1992).
[ref. S17] Herrmann, M. R.; Schenk, A. *J. Appl. Phys.* **1995**, *77*, 4522.
[ref. S18] Larcher, L. *IEEE Trans. Electron Devices***2003**, *50*, 1246.
[ref. S19] Padovani, A. Proc. *IEEE Int. Rel. Phys. Symp.***2008**, *55*, 616.
[ref. S20] Yang, N.; Henson, W. K.; Hauser, J. R.; Wortman, J. *J. IEEE Trans. Electron Devices***1999**, *46*, 1464.
[ref. S21] Duke, C. B. *Academic Press,* **1969**.
[ref. S22]Larcher, L.; Pavan, P.; Pellizzer, F.; Ghidini, G. *IEEE Trans. Electron Devices*, **2001**, *48*, 935.
[ref. S23]Sze, S. M. *Wiley-Interscience*, **1981.**
[ref. S24] Grand, D.; Bernas, A.; Amouyal, E. *Chem. Phys.***1979**, *44*, 73.
[ref. S25] Ballard, R. E. *Chem. Phy. Lett.***1972**, *16*, 300.
[ref.S26] Olympus AFM probes website for the model OMCL-AC240TM-B2, technical summary. http://probe.olympus-global.com/en/product/omcl_ac240tm_w2/ (online accessed on April 12th of 2015).